ACS Catalysis

Research Article

pubs.acs.org/acscatalysis

Mesoporous MFI Zeolite Nanosponge Supporting Cobalt Nanoparticles as a Fischer–Tropsch Catalyst with High Yield of Branched Hydrocarbons in the Gasoline Range

Jeong-Chul Kim,[†,‡] Seungyeop Lee,[†,‡] Kanghee Cho,[†] Kyungsu Na,[†] Changq Lee,[§,†] and Ryong Ryoo*[,†,§]

[†]Center for Nanomaterials and Chemical Reactions, Institute for Basic Science (IBS), Daejeon 305-701, Republic of Korea

[‡]Graduate School of Nanoscience and Technology, KAIST, Daejeon 305-701, Republic of Korea

[§]Department of Chemistry, KAIST, Daejeon 305-701, Republic of Korea

Supporting Information

ABSTRACT: A zeolite nanosponge was obtained by a seed-assisted hydrothermal synthesis route using $C_{22}H_{45}-N^+(CH_3)_2-C_6H_{12}-N^+(CH_3)_2-C_6H_{13}$ as the structure-directing agent. The zeolite was composed of disordered network of 2.5-nm-thick MFI zeolite nanolayers having a narrow distribution of mesopore diameters centered at 4 nm. The highly mesoporous texture (mesopore volume = 0.5 $cm^3\ g^{-1}$) was suitable for supporting cobalt nanoparticles with a narrow distribution of particle diameters centered at 4 nm. The Co/MFI zeolite exhibited high stability of the Co nanoparticles against particle growth, and there was accordingly high catalytic conversion of carbon monoxide to hydrocarbons and long catalytic lifetime in the Fischer–Tropsch synthesis. Furthermore, the Co/MFI catalyst exhibited high selectivity for branched hydrocarbons in the gasoline range (C_5-C_{11}), compared to conventional alumina-based catalysts. This high selectivity could be attributed to hydroisomerization in the extremely thin zeolite frameworks that provided short diffusion path lengths for branched hydrocarbons.

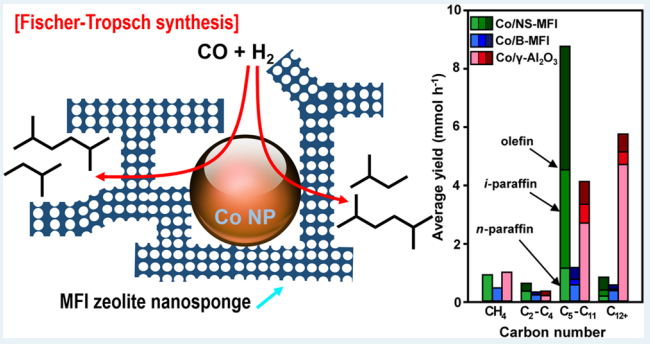

KEYWORDS: *Fischer–Tropsch synthesis, bifunctional catalyst, hierarchical zeolite, uniform mesopore diameter, high cobalt dispersion, high gasoline yield*

1. INTRODUCTION

Fischer–Tropsch (FT) synthesis is a catalytic process that produces hydrocarbons from a mixture of H_2 and CO, which is referred to as "synthesis gas" or "syngas".[1] Syngas can be readily obtained by steam reforming of natural gas, coal, and biomass.[2,3] The FT process was industrialized early in Germany as a method of transforming abundant coal into a hydrocarbon source, which addresses its lack of domestic petroleum resources.[4] Germany built nine FT plants by the end of World War II, but since then, almost all FT plants closed as crude oil became available at a much lower cost than hydrocarbons produced via FT synthesis. In recent years, however, the price of oil increased dramatically. Besides, syngas production from shale gas is anticipated to be cost competitive in the near future. These factors have led to renewed interest in the FT process.[5] SASOL has been implementing a FT-based process over the past several decades, and is currently planning to increase its operational capacity to 34 000 barrels per day.[6] Shell has also been operating an FT plant in Malaysia with a daily capacity of 14 700 barrels.[6]

In the FT synthesis process, late transition metals such as iron, ruthenium, and cobalt are used as catalysts.[7] These metals strongly interact with carbon monoxide (CO) on their surfaces and, therefore, activate the dissociation of CO for consecutive hydrogenation into hydrocarbons. Among such metal catalysts, cobalt is the most widely used because of its low cost, high CO conversion activity, and high selectivity of long-chain linear hydrocarbons (i.e., liquid fuels).[5] FT synthesis is a structure-sensitive reaction, exhibiting maximum catalytic activity in the range of 4–6 nm cobalt particle diameters.[8,9] The catalytic conversion and selectivity for long-chain hydrocarbons decreases drastically as the particle size decreases below this range. On the other hand, if the particle diameter increases beyond 6 nm, the metal dispersion decreases, and consequently, the weight-specific activity of the cobalt decreases. To obtain the optimum particle size, cobalt is often supported on γ-Al_2O_3, SiO_2, and TiO_2 with high specific surface areas.[10] Among these oxide supports, γ-Al_2O_3 has been the material most commonly adopted to date, since it has the advantage of low production cost, large external surface area, and strong metal–support interaction.[4] High-surface γ-Al_2O_3 samples supporting cobalt nanoparticles of optimum diameters showed

Received: March 2, 2014
Revised: September 22, 2014
Published: September 24, 2014

   dx.doi.org/10.1021/cs500784v | ACS Catal. 2014, 4, 3919–3927

high catalytic activity in FT synthesis. However, Co/γ-Al_2O_3 catalysts exhibited a nonselective distribution of product hydrocarbon chain lengths, according to the Anderson–Schulz–Flory (ASF) model.[6] Recently, Tao et al. reported that the product selectivity could be enhanced to a desired range of chain lengths when zeolites (a family of crystalline microporous aluminosilicates) were used as supports for cobalt nanoparticles.[11−13] This result was explained by hydrocracking of the hydrocarbon intermediates to desirable chain lengths in zeolite micropores having strong acid properties. However, the zeolite-based catalyst exhibited much lower CO conversion compared to the conventional alumina-based catalyst. This low activity was due to low metal dispersion (i.e., exceedingly large metal particles) on the limited area of zeolite external surfaces.[14]

In order to resolve the disadvantage of conventional zeolites as the metal–supporting material, Sartipi et al.[15,16] generated mesopores in an MFI zeolite through an alkali treatment. The resultant zeolite exhibited improved dispersion of cobalt, because of the large surface area of the mesopore walls. Hence, using a mesoporous zeolite to support cobalt nanoparticles led to high catalytic activity in the FT synthesis. In addition, the mesoporous Co/MFI catalyst had the advantage of low production of short-chain hydrocarbons ($<C_4$), compared with bulk Co/MFI. This result was explained by the rapidly escaping diffusion of hydrocarbon products before overcracking. Recently, Kang et al.[17,18] reported that mesoporous MFI and beta zeolites could support ruthenium nanoparticles with high metal dispersion, as an FT catalyst for the high yield of gasoline-range hydrocarbons.

In 2009, our group reported the direct synthesis of mesoporous zeolites using multiammonium surfactants as a structure-directing agent (SDA), which generated mesopores and micropores simultaneously.[19] Using the synthesis strategy, we obtained an MFI zeolite exhibiting a morphology of 2.5-nm-thick nanosheets. The MFI nanosheets were stacked regularly to form multilayers supported by surfactants, or they were assembled irregularly into a loose stacking of separate layers, depending on the synthesis conditions.[20] The former (multilamellar assembly) lost most of its interlayer spacing due to collapse when the surfactant was removed by calcination. On the other hand, the latter (unilamellar assembly) maintained the mesoporosity between neighboring nanosheets; however, the mesopore diameters were widely distributed within a range from 4 nm to 30 nm. Recently, Jo et al.[21] added MFI zeolite crystals into a synthesis composition for MFI zeolite nanosheets. The bulk crystal seeding reduced the zeolite crystallization time remarkably. More importantly, the crystal seeding gave rise to the formation of nanosheets exhibiting a nanosponge-like morphology, which had a very narrow distribution of pore diameters centered at 4 nm.

In this work, we noted the potential of the MFI zeolite nanosponge as a catalyst support. In particular, we expected that MFI zeolite frameworks with uniform mesopore diameters would have a remarkable merit as a catalyst support in bifunctional catalytic applications requiring both metal nanoparticles about the diameter of the MFI mesopores and strong acidity of the MFI zeolite frameworks. For this reason, we investigated the MFI nanosponge as a supporting material of cobalt nanoparticles for FT synthesis reaction. The dispersion of cobalt nanoparticles supported on the MFI nanosponge was measured by high-resolution transmission electron microscopy (TEM). The FT synthesis reaction was performed using the Co/MFI nanosponge as a catalyst, in comparison with bulk Co/MFI and alumina-based conventional FT catalyst. The catalytic performances were evaluated, focusing on the total CO conversion and the product selectivity for branched hydrocarbons in the gasoline range.

2. EXPERIMENTAL SECTION

2.1. Catalyst Preparation. The MFI zeolite nanosponge was hydrothermally synthesized, using [$C_{22}H_{45}$–$N^+(CH_3)_2$–C_6H_{12}–$N^+(CH_3)_2$–$C_6H_{13}(Br^-)_2$] (abbreviated hereafter as "$C_{22\text{-}6\text{-}6}$") as the zeolite SDA, and calcined bulk MFI zeolite as crystal seeds. The concept of the zeolite synthesis was the same as that of the previous method reported by Jo et al.[21] However, the details of synthesis procedure was somewhat modified. Water glass (29 wt % SiO_2, Si/Na = 1.75, Shinheung Chemical) was used as silica source instead of tetraethylorthosilicate (TEOS). The order of mixing synthesis reagents was also changed. In detail, $C_{22\text{-}6\text{-}6}$ was dissolved in distilled water. This solution was added into another solution dissolving aluminum sulfate [$Al_2(SO_4)_3{\cdot}18H_2O$, 98%, Sigma–Aldrich]. This mixture was stirred and the water glass was added into this mixture dropwise. The resultant gel was heated to 333 K and stirred for 2 h, and then the pH of this gel was adjusted to ∼10 via the addition of 10 wt % sulfuric acid solution. This gel had a molar composition of 95 SiO_2, 0.95 Al_2O_3, 7.5 $C_{22\text{-}6\text{-}6}$, 30 Na_2O, 21 H_2SO_4, 5000 H_2O. It was stirred for 6 h at 333 K and, subsequently, a commercial ZSM-5 zeolite (Zeolyst, CBV 8014, Si/Al = 40) amounting to 5 wt % of the total silica source was added as a seed into this gel. The composition of the final synthetic gel was 100 SiO_2, 1 Al_2O_3, 7.5 $C_{22\text{-}6\text{-}6}$, 30 Na_2O, 21 H_2SO_4, 5000 H_2O. This synthetic gel was stirred for 6 h further at 333 K. The synthesis gel was then heated in a Teflon-lined stainless autoclave at 423 K with tumbling for 2.5 d. The zeolite product was filtered, washed by distilled water, and dried in an oven at 373 K.

Bulk MFI zeolite was synthesized using tetrapropylammonium hydroxide (TPAOH, 10 wt %) as the zeolite SDA, following a procedure described elsewhere.[22] Aluminum sulfate and TPAOH were dissolved in distilled water, and subsequently, TEOS was added to this solution under magnetic stirring. The resultant mixture had a molar composition of 100 SiO_2, 1 Al_2O_3, 30 TPAOH, 3 H_2SO_4, 6000 H_2O. This mixture was heated in a Teflon-lined stainless autoclave at 443 K with tumbling for 3 d. The zeolite product was filtered, washed by distilled water, and dried in an oven at 373 K.

All the zeolite samples (both nanosponge and bulk) were calcined in air at 823 K. After calcination, the zeolites were slurried in a 1 M NH_4NO_3 aqueous solution a total of three times for the ion exchange to NH_4^+. The NH_4^+-exchanged zeolites were calcined again in air at 823 K for conversion to the H^+-ionic form. In addition to the zeolites, a γ-Al_2O_3 sample was purchased from Sasol (PURALOX, 98%, S_{BET} = 170 $m^2\ g^{-1}$), and supported with Co without further treatments. The Co supporting on γ-Al_2O_3, bulk MFI and nanosponge MFI zeolites was carried out by incipient wetness impregnation using an aqueous solution of cobalt nitrate [$Co(NO_3)_2{\cdot}6H_2O$, Fluka]. Typically, 0.273 g of $Co(NO_3)_2{\cdot}6H_2O$ was impregnated in 0.5 g supporting material, to provide 10 wt % Co content in the final catalyst. All Co-containing samples were dried in a convection oven at 373 K for 12 h and calcined by O_2 (99.9%, flow rate = 400 $cm^3\ min^{-1}\ g^{-1}$) at 573 K for 4 h.

2.2. Characterization. Powder X-ray diffraction (XRD) patterns were measured with a Rigaku Multiflex diffractometer

dx.doi.org/10.1021/cs500784v | ACS Catal. 2014, 4, 3919−3927

equipped with Cu Kα radiation (30 kV, 40 mA). The Ar sorption isotherms were measured at liquid Ar temperature (87 K) with a volumetric Micromeritics Model ASAP-2020 instrument. Si/Al ratios were determined by inductively coupled plasma–atomic emission spectroscopy (ICP/AES), using an OPTIMA 4300 DV instrument (Perkin–Elmer). Scanning electron microscopy (SEM) micrographs were obtained, using a Verios SEM system operating at 1 kV (decelerating voltage of 3.0 kV) without a metal coating. Transmission electron microscopy (TEM) micrographs were obtained using an aberration-corrected Titan ETEM G^2 system at an operating voltage of 300 kV.

The concentration of Brönsted acid sites was analyzed with respect to the acid strength, following a ^{31}P NMR spectroscopic method using trimethylphosphine oxide as a probe molecule.[23,24] The ^{31}P NMR chemical shift was used as an index for acid strength while the peak intensity was measured for quantification of acid sites. The NMR spectra were acquired in a solid state with 10-kHz magic angle spinning (MAS) using a Bruker Model AVANCE 400WB spectrometer at room temperature. H_2-temperature-programmed reduction (TPR) profiles were obtained using a Micromeritics AutoChem II 2920 instrument equipped with a thermal conductivity detector (TCD). For the measurement, 50 mg of each sample was loaded in a quartz U-tube. The sample was degassed at 373 K for 2 h under helium gas flow (flow rate = 50 cm^3 min^{-1}). The gas flow then was switched to a H_2-argon mixture (H_2:Ar = 1:9 in moles) at the flow rate of 50 cm^3 min^{-1}. The amount of H_2 consumption by reduction was measured by TCD, while the temperature increased from 373 K to 1173 K with the ramping rate of 10 K min^{-1}.

2.3. Catalytic Measurements. FT synthesis was carried out in a stainless steel fixed-bed reactor (7 mm inside diameter), using 0.5 g of cobalt-loaded catalysts. Prior to the FT reaction, the catalyst was reduced by high-purity H_2 (99.999%, flow rate = 50 cm^3 min^{-1}) at 673 K for 12 h. The temperature was decreased to room temperature under the H_2 flow. The gas flow then was switched to a syngas–argon mixture (H_2:CO:Ar = 6:3:1 in moles). Argon also was mixed in the reactant stream, as an internal standard for product analysis by gas chromatography (GC). The pressure of the reactant gas mixture was increased to 20 bar, then the flow rate was maintained at 20 cm^3 min^{-1}. The reaction temperature was increased to 493 K under this flow. During the reaction, gas-phase products were analyzed using an online gas chromatograph equipped with a flame ionization detector and a thermal conductivity detector. The gas products were separated using a Gaspro (Agilent) column and a Porapak Q (Supelco) column in parallel. At the same time, the liquid-phase products were collected in a cold trap (278 K) for 100 h of the reaction, and analyzed using a gas chromatograph equipped with an HP-1 column (Agilent).

3. RESULTS AND DISCUSSION

3.1. MFI Zeolite Nanosponge as a Support for Cobalt Nanoparticles. Figure 1 shows a representative SEM image, TEM image and XRD pattern of the MFI zeolite nanosponge sample, which was synthesized using $C_{22\text{-}6\text{-}6}$ and zeolite seeds. The zeolite exhibited a nanosponge-like overall morphology. The individual framework of the nanosponge had a short and narrow nanosheet-like morphology, composed of the crystalline MFI zeolite structure. The zeolitic nanosheets had a very uniform thickness of 2.5 nm along the crystal *b*-axis, with

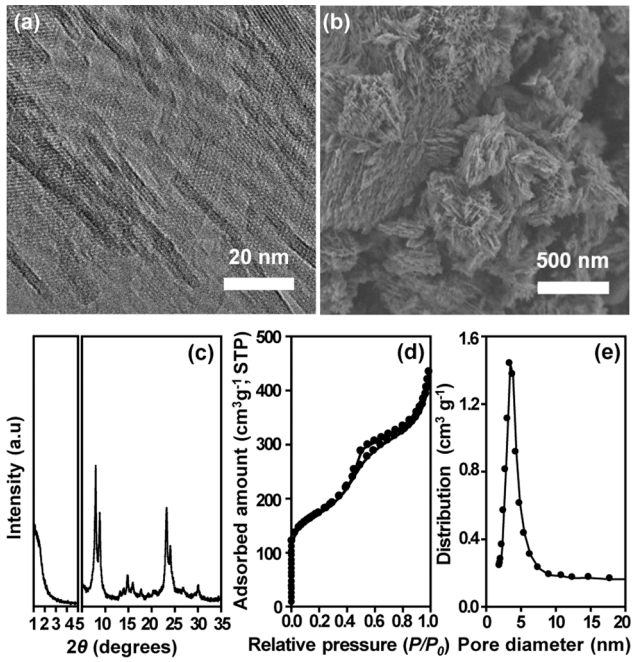

Figure 1. MFI zeolite nanosponge synthesized using $C_{22\text{-}6\text{-}6}$ surfactant as zeolite-structure directing agent and bulk MFI seed: (a) TEM image, (b) SEM image, (c) XRD pattern, (d) Ar sorption isotherm obtained at 87 K, and (e) BJH pore size distribution corresponding to the adsorption branch.

somewhat preferred orientation in parallel. These zeolite nanosheets were interconnected into a three-dimensional disordered network with very uniform interlayer spacing (~6.3 nm), as judged from the TEM image and a low-intensity XRD peak appearing at 1.4° 2θ. Despite the uniform thickness, uniform spacing, and preferred orientation, there were no distinct long-range orders between the nanosheets. This zeolite sample is designated as NS-MFI, meaning "nanosponge of MFI zeolite". In contrast to this NS-MFI sample, a conventional zeolite sample that was synthesized using tetrapropyl ammonium as an SDA exhibited bulk crystal-like particle morphologies with smooth facets (see Figure S1 in the Supporting Information). The diameters of the particles ranged from 500 nm to 1 μm. TEM images and selected-area electron diffraction patterns indicated that the particles were mostly single crystals of MFI zeolite. This latter MFI zeolite sample is designated as B-MFI, where "B" stands for "bulk". The Si/Al ratio of the two synthesized zeolites and their Brönsted acidic properties (obtained by ^{31}P NMR analysis after trimethylphosphine oxide adsorption) are summarized in Table 1. The results indicate that B-MFI and NS-MFI have similar Al contents (Si/Al = 46 and 48 for B-MFI and NS-MFI, respectively), and also similar Brönsted acid concentrations and strengths (see Figure S2 in the Supporting Information provides details of the ^{31}P NMR analysis after trimethylphosphine adsorption).[23,24]

Argon adsorption isotherms of B-MFI and NS-MFI at 87 K are shown in Figure 1. The adsorption isotherm of NS-MFI exhibits a very sharp increase in the low-pressure region of $P/P_0 < 0.1$, and a second jump in the medium-pressure region of $0.4 < P/P_0 < 0.5$. The first increase can be interpreted as argon filling in the zeolite micropores, while the second jump is attributed to the capillary condensation in mesopores between zeolite nanosheets. The adsorption isotherm in the region of $P/P_0 < 0.1$ was analyzed using nonlocal density functional theory.

dx.doi.org/10.1021/cs500784v | ACS Catal. 2014, 4, 3919–3927

Table 1. Physicochemical Properties of NS-MFI, B-MFI, and γ-Al_2O_3 Samples

catalyst	Si/Al[a]	S_{BET}[b] ($m^2\ g^{-1}$)	S_{ext}[c] ($m^2\ g^{-1}$)	V_{micro}[d] ($cm^3\ g^{-1}$)	V_{meso}[e] ($cm^3\ g^{-1}$)	BA_{tot}[f] ($\mu mol\ g^{-1}$)
NS-MFI	46	630	460	0.04	0.51	167
B-MFI	48	320	40	0.12	0.06	185
γ-Al_2O_3	n/a[g]	170	170	n/d[h]	0.45	n/d[h]

[a]Si/Al mole ratio obtained from ICP/AES analysis. [b]S_{BET} is the BET surface area obtained from Ar adsorption in relative pressure range (P/P_0) of 0.05−0.20. [c]S_{ext} is the external surface area, determined according to the *t*-plot method. [d]V_{micro} is the micropore volume calculated from *t*-plot method. [e]V_{meso} is the mesopore volume, which is calculated by subtracting V_{micro} from the total pore volume. [f]BA_{tot} is the concentration of Brönsted acid sites measured by ^{31}P NMR analysis after trimethylphosphine oxide adsorption. [g]Not applicable. [h]Not determined.

This analysis showed a sharp distribution of pore diameters centered at 0.55 nm, which is in good agreement with the micropore diameter of the MFI zeolite (0.53 × 0.56 nm and 0.51 × 0.55 nm). The adsorption isotherm in the region of $0.4 < P/P_0 < 0.9$ was analyzed using the Barrett−Joyner−Halenda (BJH) algorithm, which resulted in a narrow distribution of mesopore diameters that peaked at 4 nm. The mesopore volume of the NS-MFI zeolite was 0.5 $cm^3\ g^{-1}$ (Table 1). This is comparable to the mesopore volume (0.6 $cm^3\ g^{-1}$) of ordered mesoporous MCM-41 silica with similar pore diameters (~4.1 nm).[25] The NS-MFI zeolite had a high specific BET surface area (S_{BET} = 630 $m^2\ g^{-1}$, Table 1), and an external surface area of 460 $m^2\ g^{-1}$ (determined by the *t*-plot method). This result was in good agreement with the large area of mesopore walls in the highly mesoporous texture. Compared to the mesoporous NS-MFI zeolite, B-MFI had a very small volume of mesopores (0.06 $cm^3\ g^{-1}$). The pore size distribution analysis confirmed the sole presence of micropores with a very uniform diameter of 0.55 nm (see Figure S1 in the Supporting Information). The BET area for B-MFI was much smaller (320 $m^2\ g^{-1}$) than that for NS-MFI, and the external surface area was almost negligible (40 $m^2\ g^{-1}$).

In order to evaluate the catalytic performance in the FT synthesis reaction, the NS-MFI zeolite was supported with 10 wt % cobalt. The cobalt supporting process consisted of incipient-wetness impregnation of $Co(NO_3)_2$ aqueous solution, and the subsequent calcination to convert $Co(NO_3)_2$ to a cobalt oxide. The NS-MFI zeolite supported with Co is designated as "Co/NS-MFI". For comparison, B-MFI was supported with 10 wt % Co in the same manner. This sample is denoted as "Co/B-MFI". A commercially available γ-alumina sample with high specific surface area (S_{BET} = 170 $m^2\ g^{-1}$) was also supported with 10% wt Co and is denoted by Co/γ-Al_2O_3. Figure 2 shows the XRD patterns of the three samples supporting 10 wt % Co species after calcination. The XRD patterns exhibited diffraction peaks centered at 2θ = 30°, 37°, 45°, and 59°, which correspond to Co_3O_4 of the spinel structure.[26] No reflection peaks for other cobalt species were detected by XRD. Thus, the XRD indicated that the cobalt nitrate was completely converted to the spinel Co_3O_4 by calcination in O_2. Figure 3 shows representative TEM images of the Co/NS-MFI, Co/B-MFI, and Co/γ-Al_2O_3 samples. In the case of Co/NS-MFI, the cobalt was supported as tiny nanoparticles (black spots). The nanoparticle diameters were estimated using Digital Micrograph software distributed by Gatan, using several TEM images showing more than 20 zeolite particles in total. The distribution of the particle diameters obtained in this manner was quite narrowly peaked at ~4 nm. The mode value of the particle diameters (4 nm) was the same as the mesopore diameters in the NS-MFI zeolite. Compared to the uniform Co nanoparticles supported on NS-MFI, the Co/B-MFI sample exhibited a wide distribution of Co particle

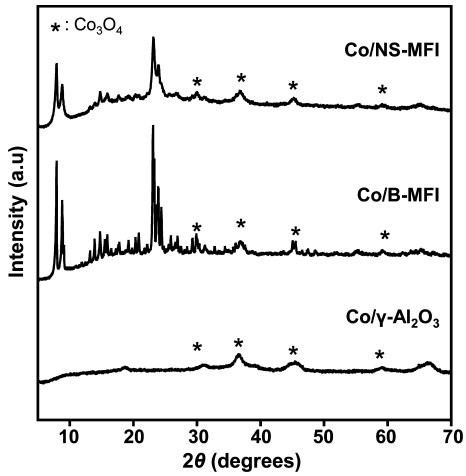

Figure 2. Powder XRD patterns of the Co/NS-MFI, Co/B-MFI, and Co/γ-Al_2O_3 catalysts.

diameters over 10−20 nm. The particles were located on the external surfaces (Figure 3). This result indicates that the mesopores in NS-MFI were preferred locations of Co nanoparticles. The locations may be attributed to the large external surfaces of the zeolite nanosheets that are terminated by numerous silanol groups. The polarity of the silanol groups may induce interactions to retain the cobalt species.

A TPR analysis was performed for Co/NS-MFI, in order to investigate the interactions between the support and the cobalt species. This result is compared with the TPR profiles of Co/γ-Al_2O_3 and Co/B-MFI in Figure 4. All of the samples exhibited several TPR peaks over the range of 373−1173 K. Over the TPR range, temperatures below 700 K correspond to the reduction of Co oxide without significant interactions with support, while the higher temperature region is attributed to strong metal−support interactions such as electrostatic binding and covalent bonding.[27] In particular, the location of a peak appearing at a temperature of 900 K or higher can be used as an index for strong metal−support interactions. Such a peak is centered at 915 K for the case of Co/B-MFI, 1000 K for Co/NS-MFI, and 1070 K for Co/γ-Al_2O_3. As judged by the peak temperature, the metal−support interactions could be assessed to increase in the order of Co/B-MFI < Co/NS-MFI < Co/γ-Al_2O_3. From this order, it was expected that the diameters of cobalt particles would decrease in the order of Co/B-MFI > Co/NS-MFI > Co/γ-Al_2O_3. However, the actual result changed to Co/B-MFI > Co/NS-MFI ≈ Co/γ-Al_2O_3. That is, the average Co particle diameters in Co/NS-MFI and Co/γ-Al_2O_3 were very similar, despite a marked difference in the TPR profiles. Moreover, as mentioned above, the NS-MFI zeolite could support Co nanoparticles with quite similar diameters to the mesopores in the zeolite. Hence, the formation of the Co

dx.doi.org/10.1021/cs500784v | ACS Catal. 2014, 4, 3919−3927

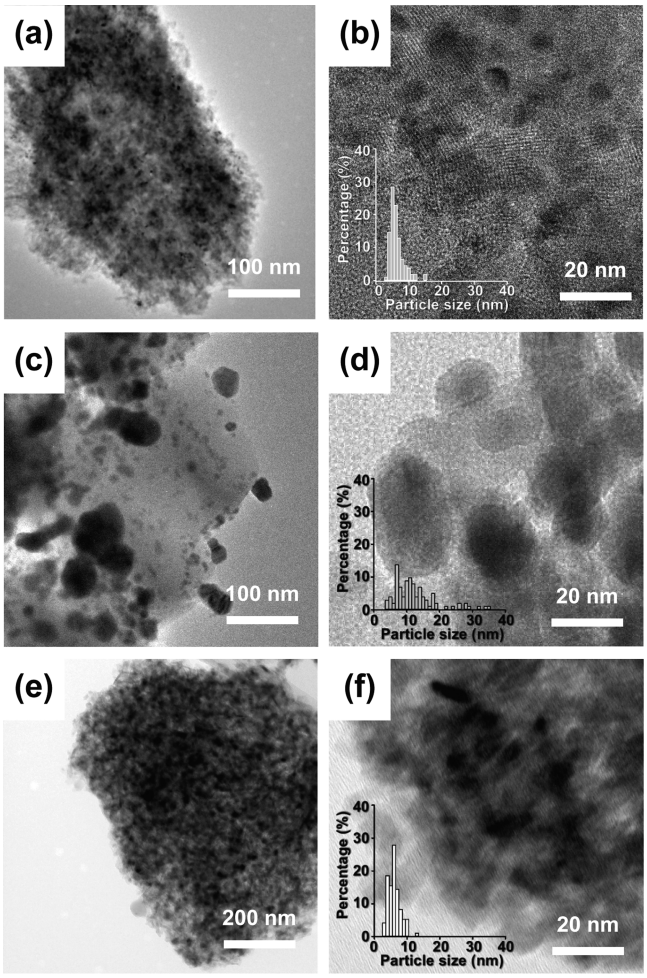

Figure 3. TEM images of (a, b) Co/NS-MFI, (c, d) Co/B-MFI, and (e, f) Co/γ-Al_2O_3 catalysts. Insets of TEM images in right column are the size distribution of cobalt nanoparticles supported on NS-MFI, B-MFI, and γ-Al_2O_3, which were derived from TEM images.

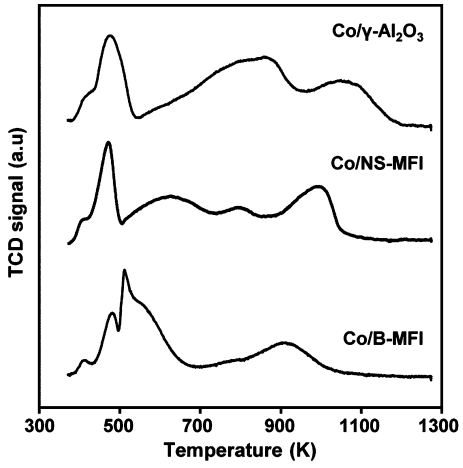

Figure 4. TPR profiles of the Co/NS-MFI, Co/B-MFI, and Co/γ-Al_2O_3 catalysts.

nanoparticles with uniform diameters in NS-MFI could be attributed to the confining effect of uniform mesopores.

3.2. Fischer–Tropsch Synthesis Reaction over Co/MFI Nanosponge. *Conversion of CO.* In this section, the catalytic performance of Co/NS-MFI is presented and, compared to that of Co/B-MFI and Co/γ-Al_2O_3. In particular, the catalytic performance is evaluated by focusing on the total conversion of CO and the product selectivity for branched hydrocarbons in the gasoline range at 493 K. The CO conversion is plotted as a function of reaction time in Figure 5. This plot shows a distinct

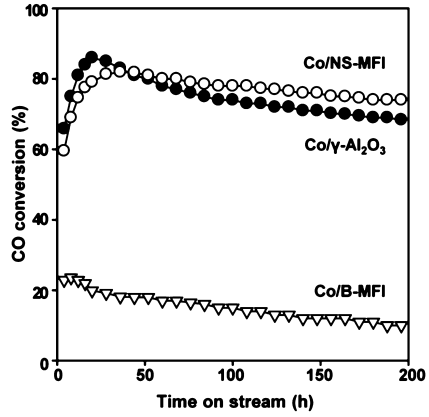

Figure 5. CO conversion over Co/NS-MFI, Co/B-MFI, and Co/γ-Al_2O_3, plotted as a function of time on stream. (Reaction conditions: GHSV = 2.4 L h^{-1} g^{-1}, reaction temperature = 493 K, reaction pressure = 20 bar, and H_2/CO ratio = 2.)

increase in the CO conversion at an early period, and subsequently, a gradual decrease after reaching a maximum point. The initial period of increase is called an "induction period", and its presence is typical for cobalt-based FT catalysts.[28,29] During the induction period, it is known that cobalt metal nanoparticles generate a surface carbide species that is catalytically more active than Co_3O_4 and Co(0) metal.[30] Therefore, the catalyst becomes progressively more active with increasing time. After this, the initial activation is followed by a gradual decrease in catalytic activity, which is normally due to the sintering of cobalt particles. As a result, the conversion plot shows a maximum CO conversion at a certain point. Figure 5 shows that the conversion at the maximum point was 23% in the case of Co/B-MFI. On the other hand, the cobalt catalyst supported on Co/NS-MFI exhibited ~4 times higher conversion (82%), which is similar to that on Co/γ-Al_2O_3 shown in Figure 5 (89%). The high CO conversion over the Co/NS-MFI catalyst means that the Co nanoparticles were supported with optimum diameters, and were stably retained in the mesopores of the hierarchical zeolite. So far, many studies on FT synthesis used zeolites as catalyst supports.[13−16] However, to the best of our knowledge, there have been no other reports of high catalytic conversions that are comparable to the γ-Al_2O_3-based catalysts. Compared with the Co/γ-Al_2O_3, the present Co/NS-MFI catalyst exhibited a slightly lower conversion of CO during the early period of reaction time, but the Co/NS-MFI was deactivated more slowly (Figure 5). As a result, the Co/NS-MFI catalyst became more active than Co/γ-Al_2O_3 when used longer than 50 h. After 200 h of reaction time, the CO conversion for Co/NS-MFI and Co/γ-Al_2O_3 are 74% and 68%, respectively. The slow deactivation of Co/NS-MFI suggested that the cobalt nanoparticles supported on the zeolite mesopore walls were more resistant to agglomeration than the cobalt particles located on an open surface of γ-Al_2O_3. To confirm this hypothesis, the diameters of the cobalt particles in the two catalyst samples were analyzed by high-resolution TEM before and after the catalytic reactions. In this analysis, the

dx.doi.org/10.1021/cs500784v | ACS Catal. 2014, 4, 3919−3927

cobalt nanoparticles (4−6 nm in diameter) supported on the NS-MFI zeolite did not show a notable change after 200 h of reaction at 493 K (Figure S3 in the Supporting Information), and also after 100 h of reaction 573 K (Figure S4 in the Supporting Information). On the other hand, the Co particle size distribution on γ-Al_2O_3 shifted to a larger size, even after the reaction at 493 K.

Product Selectivity. All of the products generated from CO by the zeolite- and alumina-based catalysts were analyzed using GC and mass spectrometry (MS). The analysis showed that the products consisted of CO_2, oxygenate compounds, and hydrocarbons with different carbon numbers. The gas products were analyzed online at various reaction times. This analysis gave the product selectivity plotted as a function of the reaction time-on-stream (see Figure S5 in the Supporting Information). To obtain an average value during the entire reaction period, the selectivity was integrated over 100 h. On the other hand, the liquid products were collected in a bottle over 100 h, and analyzed by off-line GC to determine the average selectivity. The product selectivity and conversion, which were averaged over 100 h, are presented in Table 2 and the product selectivity is plotted in Figure 6. As Table 2 shows, the Co/NS-MFI and Co/γ-Al_2O_3 catalysts exhibited very similar CO conversion. Nevertheless, the product distributions were conspicuously different. Most hydrocarbons generated over Co/NS-MFI were in the gasoline range (C_5−C_{11}), while the hydrocarbons from Co/γ-Al_2O_3 were mostly in the diesel or higher range (C_{12+}). The high selectivity to C_5−C_{11} was checked by repeating the analysis at a separate laboratory (see Table S1 and Figure S6; experimental details are provided in the Supporting Information). The high selectivity of the Co/NS-MFI catalyst to gasoline-range hydrocarbons can be attributed to the presence of strong Brönsted acid sites in the zeolite support, whereas these strong Brönsted acid sites are known to tailor long-chain hydrocarbons to shorter hydrocarbons through hydrocracking reactions. In the present work, the product selectivity of the Co/NS-MFI was analyzed at various points of the reaction time-on-stream. The result showed that the catalytic selectivity did not change significantly (see Table S2 in the Supporting Information). From the selectivity data, it is believed that the acidity of the catalyst support did not change significantly during the reaction period.

Table 2. CO Conversion over Co/NS-MFI, Co/B-MFI, and Co/γ-Al_2O_3 Samples and Resultant Product Selectivity, Which Were Averaged over a Fischer−Tropsch (FT) Reaction Time of 100 h

	Co/NS-MFI[a]	Co/γ-Al_2O_3[a]	Co/B-MFI[a]	Co/B-MFI[d]
average CO conversion (mmol h^{-1})	11.2	11.3	2.6	10.5
selectivity (C%)[b]				
CO_2	4.6	6.8	1.0	1.3
CH_4	7.9	8.1	17.1	16.3
olefin (C_2−C_4)	2.2	1.2	3.5	2.4
n-paraffin (C_2−C_4)	3.2	1.8	8.7	9.7
olefin (C_5−C_{11})	35.6	6.2	14.2	16.1
i-paraffin (C_5−C_{11})	28.4	5.1	6.7	11.3
n-paraffin (C_5−C_{11})	9.8	21.5	20.8	12.9
olefin + paraffin (C_{12+})	7.2	45.7	20.6	27.7
others[c]	1.1	3.6	7.4	2.3

[a]Reaction conditions: 0.5 g of catalyst; gas hourly space velocity, GHSV = 2.4 L h^{-1} g^{-1}; temperature, T = 493 K; pressure, P = 20 bar; H_2/CO ratio = 2; time-on-stream, 100 h. [b]Selectivity (C%) of individual component in product mixture, which were averaged over 100 h of reaction time. [c]Oxygenates and aromatic compounds, which were included in the product mixture. [d]Reaction conditions: 1.5 g of catalyst, GHSV = 0.8 L h^{-1} g^{-1}, temperature = 493 K, pressure = 20 bar, H_2/CO ratio = 2, time-on-stream, 100 h.

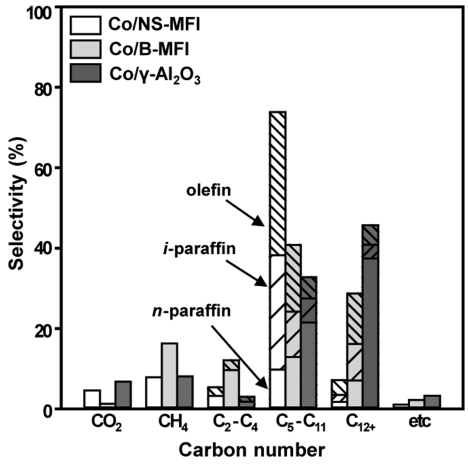

Figure 6. Product selectivity of Co/NS-MFI (0.5 g), Co/B-MFI (1.5 g), and Co/γ-Al_2O_3 (0.5 g) catalysts, which were averaged over 100 h of the FT reaction time. (Reaction conditions: flow rate of reactant mixture (H_2:CO:Ar = 6:3:1 in moles) = 20 mL min^{-1}, reaction temperature = 493 K, and reaction pressure = 20 bar.)

When Co/NS-MFI and Co/B-MFI were compared, the Co/NS-MFI catalyst exhibited markedly higher gasoline selectivity. Since the Co/B-MFI catalyst exhibited a very low conversion of CO, compared to the same amount of Co/NS-MFI, the product selectivity of Co/B-MFI was measured using three times more catalyst than Co/NS-MFI. This adjustment allowed us to compare the product selectivity of the two catalysts at similar CO conversions (i.e., 77% with Co/B-MFI, and 82% with Co/NS-MFI). The results of this selectivity analysis performed in this manner indicated that the gasoline selectivity was much higher in the case of Co/NS-MFI (73.8%) than of Co/B-MFI (40.3%). Another notable point was that Co/NS-MFI exhibited lower selectivity to methane (7.9% with Co/NS-MFI, 16.3% with Co/B-MFI) as well as other low-molecular-weight hydrocarbons in the range of C_2−C_4 (5.4% with Co/NS-MFI, 12.1% with Co/B-MFI). The low selectivity to methane and short hydrocarbons of the zeolite nanosheet-supported catalyst is desirable for gasoline production. The low selectivity to light hydrocarbons seems to be related to the very small crystal thickness. In the case of the NS-MFI catalyst, Brönsted acid sites are located at the external surfaces and on the micropore walls that are very close to the external surfaces. It is therefore reasonable that the hydrocarbon intermediates generated at these sites rapidly diffuse out before cracking occurs excessively to light hydrocarbons. Similar phenomena were reported for hydrocarbon reactions in MFI zeolites.[22] We propose that this explains why the cobalt catalyst supported on the ultrathin framework of the NS-MFI zeolite could result in such high product selectivity to the gasoline-ranged hydrocarbons.

Regarding the product selectivity within the gasoline range, *i*-paraffin selectivity increased in the order of Co/γ-Al_2O_3 < Co/B-MFI < Co/NS-MFI (see Figure 6 and Table 2). High selectivity for *i*-paraffins in the zeolite-supported catalysts

dx.doi.org/10.1021/cs500784v | ACS Catal. 2014, 4, 3919−3927

compared to the alumina-supported catalyst can be attributed to the synergistic binary catalytic functions of the supported cobalt species and the zeolite acid sites. The acid sites in zeolite can convert linear hydrocarbon intermediates to branched compounds through hydroisomerization reactions during the FT synthesis reaction on the cobalt surface.[31] Of the two zeolite-based catalysts, the Co/NS-MFI exhibited higher selectivity to *i*-paraffins. Recently, Kim et al.[22] investigated *n*-heptane hydroisomerization using MFI zeolite nanosheets supporting 1 wt % Pt nanoparticles. They reported that the selectivity for *i*-heptane increased as the framework thickness of the MFI zeolite decreased. The selectivity increase was attributed to the short diffusion path lengths in the zeolite nanosheet, so that branched products could easily escape before cracking. We checked the zeolite thickness effect of Co/NS-MFI by performing hydroisomerization of *n*-octane at 493 K (the same temperature as the FT synthesis). The result of the hydroisomerization reaction is summarized in Table S3 in the Supporting Information, and it indicates that the thin nanosheet catalyst exhibited only a slightly higher conversion of *n*-octane compared to the bulk zeolite (7.2% *n*-octane conversion over Co/NS-MFI and 5.8% over Co/B-MFI). However, there was a remarkable difference in the selectivity for branched octanes (81.0% with Co/NS-MFI, and 55.1% with Co/B-MFI). Furthermore, we checked the catalytic activity of the Co/NS-MFI for hydrocracking and hydroisomerization of *n*-hexadecane at 493 K. The result indicated that hydroisomerization and hydrocracking of the long-chain hydrocarbons could happen under the reaction conditions (see Table S4 in the Supporting Information).[16]

According to the ASF rule, the maximum C_5-C_{11} fraction is predicted to 50% when the chain growth probability is optimized. The product selectivity of Co/NS-MFI seemed to deviate from the ASF rule, but this can be interpreted as a result of the aforementioned secondary reactions, i.e., hydroisomerization and hydrocracking.[16,17,32] The high selectivity for gasoline and branched hydrocarbons in Co/NS-MFI was confirmed under various reaction conditions (temperatures and H_2/CO ratios). The results of the catalytic measurement under these conditions are summarized in Table S5 in the Supporting Information. As the results show, the Co/NS-MFI catalyst exhibited a large increase in CO conversion, from 16% to 93%, when the reaction temperature was changed from 473 K to 513 K with $H_2/CO = 2$. The CO conversion over Co/γ-Al_2O_3 also increased similarly, from 19% to 95%. However, even at such a high conversion rate, the Co/NS-MFI catalyst could exhibit much higher selectivity to branched hydrocarbons in the gasoline range. When the H_2/CO ratio changed from 2 to 1 at 493 K, both catalyst samples exhibited a sharp decrease in the CO conversion (from 82% to 16% in Co/NS-MFI and from 89% to 11% in Co/γ-Al_2O_3). Nevertheless, the Co/NS-MFI catalyst still exhibited much higher selectivity (17.4%) to the branched hydrocarbons, compared to Co/γ-Al_2O_3 catalyst (8.1%).

Comparison with Other Zeolites. As shown in the previous section, the alumina-based catalyst exhibited high CO conversion but poor product selectivity in the gasoline range. In contrast, the bulk zeolite-based catalyst exhibited high gasoline selectivity but poor CO conversion. The Co/NS-MFI catalyst had the dual advantages of both high conversion and high selectivity. In recent years, a few other reports used mesoporous MFI zeolites as metal catalyst supports for FT synthesis.[15−18] In other studies, the mesoporous MFI zeolites were prepared through post-synthetic desilication of bulk zeolite. The resultant zeolites after the generation of mesopores were supported with ruthenium or cobalt nanoparticles. The metal-supporting mesoporous zeolites were reported to show high conversion of CO as well as selectivity of branched hydrocarbons in the gasoline range, compared to the use of bulk MFI zeolite as the metal support. However, due to the difference in the FT reaction conditions, it was difficult to directly compare these previous results with the Co/NS-MFI catalyst prepared in the present study. For a direct comparison, we performed the same desilication treatment on our bulk MFI zeolite sample (see Supporting Information for the details of the desilication procedure). The desilicated zeolite prepared in this manner was denoted as "DS-MFI". The DS-MFI zeolite contained a fairly large volume of mesopores (0.18 $cm^3\ g^{-1}$; see Table S6 in the Supporting Information), but the pore size distribution was much broader than that of NS-MFI (see Figure S7 in the Supporting Information). Cobalt nanoparticles could be supported on the DS-MFI zeolite with a fairly narrow distribution of particle diameters ∼5−10 nm in size (see Figure S8 in the Supporting Information). Initially, the CO conversion of Co/DS-MFI catalyst increased to 83%, which was comparable to that of Co/NS-MFI. However, after 100 h of reaction time, the cobalt nanoparticles on DS-MFI were easily agglomerated into particles with a wide distribution of diameters of ∼5−20 nm. Consequently, the CO conversion decreased to 59% (see Figure S9 in the Supporting Information). Moreover, the DS-MFI zeolite frameworks (∼20 nm, as judged by TEM) were much thicker than the 2.5 nm nanosheet. The Co/DS-MFI catalyst exhibited 14% product selectivity to branched hydrocarbons in the gasoline range. The low selectivity seemed to be due to the framework thickness.

Recently, other types (e.g., MTW and MRE) of zeolite were synthesized with a nanosponge morphology by the synthesis strategy using multiammonium surfactants as SDAs.[33] Such MTW and MRE zeolite nanosponges were obtained in the present study, following the same synthesis procedure (see the Supporting Information). These zeolites were supported with 10% wt cobalt, for comparison with Co/NS-MFI zeolite as a catalyst in the FT synthesis reaction. Characterization of the synthesized zeolite samples using XRD, TEM, and Ar sorption analysis indicated that the samples were built by a 3D disordered assembly of 5-nm-thick zeolite frameworks (see the TEM images in Figures S10 and S11 in the Supporting Information). The mesoporous textures of the synthesized MTW and MRE zeolites were very similar to that of NS-MFI. The mesopore volumes of MTW and MRE were 0.66 $cm^3\ g^{-1}$ and 0.51 $cm^3\ g^{-1}$, respectively. The pore size distributions were sharply peaked at 4.5 nm, as in the case of the MFI nanosponge. The result from the cobalt-supporting experiment indicated that highly mesoporous structures with uniform pore diameters had the advantage of dispersing the cobalt nanoparticles with uniform diameters within the mesopores, similar to the case of Co/NS-MFI (compare Figure 3 and Figure S7 in the Supporting Information). The Co/MTW and Co/MRE catalyst samples exhibited high average CO conversions (72.2% and 70.5% over MTW and MRE, respectively; see Table 3), which were comparable to the result obtained from Co/NS-MFI. Both of the catalysts were deactivated slowly (Figure S8 in the Supporting Information). In addition, the nanosponge catalysts exhibited high selectivity to branched hydrocarbons in

dx.doi.org/10.1021/cs500784v | ACS Catal. 2014, 4, 3919−3927

Table 3. Average CO Conversion and Product Distributions for 100 h over Co/DS-MFI, Co/MTW, and Co/MRE Samples[a]

	Co/DS-MFI	Co/MTW	Co/MRE
average CO conversion (mmol h^{-1})	9.1	10.3	10.6
product distributions (C%)[b]			
CO_2	1.1	3.2	1.5
CH_4	12.2	13.5	11.9
olefin (C_2–C_4)	6.6	7.1	8.3
n-paraffin (C_2–C_4)	6.1	7.5	7.3
olefin (C_5–C_{11})	34.8	28.5	31.6
i-paraffin (C_5–C_{11})	14.0	22.0	22.0
n-paraffin (C_5–C_{11})	11.5	7.9	9.5
olefin + paraffin (C_{12+})	13.7	9.0	7.1
others[c]	0.3	1.3	0.8

[a]Reaction conditions: 0.5 g of catalyst; GHSV = 2.4 L h^{-1} g^{-1}; temperature, T = 493 K; pressure, P = 20 bar; H_2/CO ratio = 2; time-on-stream = 100 h. [b]Selectivity (C%) of individual component in product mixture, which were averaged over 100 h of reaction time. [c]Oxygenates and aromatic compounds, which were included in the product mixture.

the gasoline range (22% for both Co/MTW and Co/MRE; see Table 3).

4. CONCLUSIONS

We were able to synthesize an MFI zeolite nanosponge, following a recently developed zeolite synthesis strategy that uses hierarchical structure-directing surfactants and seeding for the zeolite crystallization. The zeolite nanosponge was composed of ultrathin zeolite walls that were irregularly interconnected into a three-dimensional mesoporous network. The mesopore diameters were quite uniform, despite the disordered pore arrangement. This zeolite nanosponge exhibited the remarkable advantage of supporting cobalt nanoparticles with uniformly controlled particle sizes by the mesopore diameters. With optimum particle diameters, the cobalt-supporting zeolite nanosponges could have high catalytic performance in an FT synthesis reaction. The confined cobalt particles exhibited high resistance to sintering. This was why the catalyst exhibited high conversion of CO and long catalytic lifetime. In addition, the thin zeolitic walls provided the advantage of high selectivity to branched hydrocarbons in the gasoline range (probably due to the diffusion effect). Recent studies show that the present synthesis strategy can be extended to other zeolites, including MTW and MRE. The mesopore diameters of the zeolites can be tailored to a desired size by choosing a surfactant with a different tail length, and also by adding a pore-expanding agent. Such zeolite nanosponges may provide new opportunities as advanced catalysts for various bifunctional catalytic applications that require both high dispersion of metal/metal oxide nanoparticles and strong acidity of zeolite frameworks.

■ ASSOCIATED CONTENT

Supporting Information

Detailed procedures for post-synthetic desilication of MFI, and the synthesis of MTW and MRE zeolite nanosponges have been provided. Additional results from the characterization of the FT catalysts and the investigation of FT synthesis reaction have been provided. The catalytic results by SK Innovation Company have been provided. This material is available free of charge via the Internet at http://pubs.acs.org.

■ AUTHOR INFORMATION

Corresponding Author

*Tel.: +82 42 350 2830. Fax: +82 42 350 8130. E-mail: rryoo@kaist.ac.kr.

Notes

The authors declare no competing financial interest.

■ ACKNOWLEDGMENTS

This work was supported by Grant No. IBS-R004-D1. The authors are grateful to SK Innovation, for providing access to catalysis test facilities for independent checking.

■ REFERENCES

(1) Dry, M. In *Handbook of Heterogeneous Catalysis*, Vol. *6*; Ertl, G., Knözinger, H., Schüth, F., Weitkamp, J., Eds.; Wiley–VCH: Weinheim, Germany, 2008; pp 2965–2994.
(2) Dry, M. *Catal. Today* **2002**, *71*, 227–241.
(3) van Steen, E.; Claeys, M. *Chem. Eng. Technol.* **2008**, *31*, 655–666.
(4) Leckel, D. *Energy Fuels* **2009**, *23*, 2342–2358.
(5) Khodakov, A. Y.; Chu, W.; Fongarland, P. *Chem. Rev.* **2007**, *107*, 1692–1744.
(6) Vandeloosdrecht, J.; Balzhinimaev, B.; Dalmon, J.; Niemantsverdriet, J.; Tsybulya, S.; Saib, a; Vanberge, P.; Visagie, J. *Catal. Today* **2007**, *123*, 293–302.
(7) Henrici-Olivé, G.; Olivé, S. *Angew. Chem., Int. Ed.* **1976**, *15*, 136–141.
(8) Bezemer, G. L.; Bitter, J. H.; Kuipers, H. P. C. E.; Oosterbeek, H.; Holewijn, J. E.; Xu, X.; Kapteijn, F.; van Dillen, A. J.; de Jong, K. P. *J. Am. Chem. Soc.* **2006**, *128*, 3956–3964.
(9) den Breejen, J. P.; Radstake, P. B.; Bezemer, G. L.; Bitter, J. H.; Frøseth, V.; Holmen, A.; de Jong, K. P. *J. Am. Chem. Soc.* **2009**, *131*, 7197–7203.
(10) Storsater, S.; Totdal, B.; Walmsley, J.; Tanem, B. *J. Catal.* **2005**, *236*, 139–152.
(11) Sun, B.; Qiao, M.; Fan, K.; Ulrich, J.; Tao, F. F. *ChemCatChem.* **2011**, *3*, 542–550.
(12) Zhang, Q.; Kang, J.; Wang, Y. *ChemCatChem.* **2010**, *2*, 1030–1058.
(13) Zhang, Q.; Cheng, K.; Kang, J.; Deng, W.; Wang, Y. *ChemSusChem* **2014**, *7*, 1251–1264.
(14) Bessell, S. *Appl. Catal., A* **1993**, *96*, 253–268.
(15) Sartipi, S.; Parashar, K.; Makkee, M.; Gascon, J.; Kapteijn, F. *Catal. Sci. Technol.* **2013**, *3*, 572–575.
(16) Sartipi, S.; Parashar, K.; Valero-Romero, M. J.; Santos, V. P.; van der Linden, B.; Makkee, M.; Kapteijn, F.; Gascon, J. *J. Catal.* **2013**, *305*, 179–190.
(17) Kang, J.; Cheng, K.; Zhang, L.; Zhang, Q.; Ding, J.; Hua, W.; Lou, Y.; Zhai, Q.; Wang, Y. *Angew. Chem., Int. Ed.* **2011**, *50*, 5200–5203.
(18) Cheng, K.; Kang, J.; Huang, S.; You, Z.; Zhang, Q.; Ding, J.; Hua, W.; Lou, Y.; Deng, W.; Wang, Y. *ACS Catal.* **2012**, *2*, 441–449.
(19) Choi, M.; Na, K.; Kim, J.; Sakamoto, Y.; Terasaki, O.; Ryoo, R. *Nature* **2009**, *461*, 246–249.
(20) Na, K.; Park, W.; Seo, Y.; Ryoo, R. *Chem. Mater.* **2011**, *23*, 1273–1279.
(21) Jo, C.; Cho, K.; Kim, J.; Ryoo, R. *Chem. Commun.* **2014**, *50*, 4175–4177.
(22) Kim, J.; Kim, W.; Seo, Y.; Kim, J.-C.; Ryoo, R. *J. Catal.* **2013**, *301*, 187–197.
(23) Seo, Y.; Cho, K.; Jung, Y.; Ryoo, R. *ACS Catal.* **2013**, *3*, 713–720.
(24) Lunsford, J. H.; Rothwell, W. P.; Shen, W. *J. Am. Chem. Soc.* **1985**, *107*, 1540–1547.

(25) Kruk, M.; Jaroniec, M.; Kim, J. M.; Ryoo, R. *Langmuir* **1999**, *15*, 5279−5284.
(26) Li, X.; He, J.; Meng, M.; Yoneyama, Y.; Tsubaki, N. *J. Catal.* **2009**, *265*, 26−34.
(27) Arnoldy, P.; Moulijn, J. A. *J. Catal.* **1985**, *93*, 38−54.
(28) Iglesia, E.; Soled, S. L.; Fiato, R. A. *J. Catal.* **1992**, *137*, 212−224.
(29) Song, D.; Li, J. *J. Mol. Catal. A: Chem.* **2006**, *247*, 206−212.
(30) Davis, B. H. *Fuel Process. Technol.* **2001**, 157−166.
(31) Bessell, S. *Appl. Catal., A* **1995**, *126*, 235−244.
(32) Li, X.-G.; Liu, C.; Sun, J.; Xian, H.; Tan, Y.-S.; Jiang, Z.; Taguchi, A.; Inoue, M.; Yoneyama, Y.; Abe, T.; Tsubaki, N. *Sci. Rep.* **2013**, *3*, 2813−2818.
(33) Kim, W.; Kim, J.-C.; Kim, J.; Seo, Y.; Ryoo, R. *ACS Catal.* **2013**, *3*, 192−195.